A Combined Spectroscopic and Theoretical Analysis of Plasmonic Silver Nanoparticles Sensor Towards Detailed Microscopic Understanding of Heavy Metal Detection

Nivedita Pan
S N Bose National Centre for Basic Sciences
Tuhin Kumar Maji
S N Bose National Centre for Basic Sciences
Sayantika Banarjee
Sister Nivedita University
Pritam Biswas
Techno International New Town
Arka Chatterjee
S N Bose National Centre for Basic Sciences
Mala Mitra
Techno International New Town
Arpita Chatterjee
Techno International New Town
Dr Samir Kumar Kumar Pal (skpal@bose.res.in)
S N Bose National Centre for Basic Sciences https://orcid.org/0000-0001-6943-5828

Research Article

Keywords: Silver nanoparticles, Localized Surface Plasmon Resonance, Self-assembled nanoparticles, Aggregation, Theoretical modelling, Lead pollution

Posted Date: March 19th, 2021

DOI: https://doi.org/10.21203/rs.3.rs-216756/v1

Version of Record: A version of this preprint was published at Plasmonics on August 6th, 2021. See the published version at https://doi.org/10.1007/s11468-021-01514-6.

A Combined Spectroscopic and Theoretical Analysis of Plasmonic Silver Nanoparticles Sensor Towards Detailed Microscopic Understanding of Heavy Metal Detection

Nivedita Pan[1], Tuhin Kumar Maji[1], Sayantika Banarjee[2], Pritam Biswas[3], Arka Chatterjee[1], Mala Mitra*[,3], Arpita Chatterjee*[,3], and Samir Kumar Pal*[,1]

[1] *Department of Chemical, Biological and Macromolecular Sciences,*

S. N. Bose National Centre for Basic Sciences,

Block JD, Sector III, Salt Lake,

Kolkata 700 106, India

[2]*Department of Physics,*

Sister Nivedita University,

DG 1/2 New Town,

Kolkata 700 156, India

[3] *Department of Basic Science and Humanities*

Techno International New Town

Block - DG 1/1, Action Area 1

New Town, Rajarhat,

Kolkata 700156, India

*Corresponding Authors Email: skpal@bose.res.in (S. K. Pal), arpita.chattopadhyay@gmail.com (A. Chatterjee), mala.mitra@tict.edu.in (M. Mitra)

Acknowledgements

N.P. and T.K.M. would like to thank DST for fellowship. We thank Probir Kumar Sarkar, Ananda Mohan College, India for discussion. We thank DST, India for Abdul Kalam Technology Innovation National Fellowship (INAE/121/AKF).

Abstract

Plasmonic nanoparticles are of great importance owing to their highly responsive 'Localized Surface Plasmon Resonance' (LSPR) behaviour to self-agglomeration/ aggregation leading to the development of various nanosensors. Herein we demonstrated the definite self-assembly of citrate functionalized silver nanoparticles (AgNPs) into a one-dimensional linear chain in presence of charged lead ions (Pb^{2+}), one of the most toxic heavy metal pollutants. We have explored detail mechanism using a variety of spectroscopic tools and electron microscopy. The self-aggregation of AgNPs leads to the generation of new LSPR modes due to coupling of nearby existing modes. The conclusion of our experimental findings is duly supported by our developed numerical modelling based on the quasi-static approximation that the generated new LSPR modes are solely due to formation of chain-like aggregation of AgNPs. We have also monitored the LSPR spectra in presence of other metal ions, however, only Pb^{2+} found to give such unique self-assembled geometry may due to its high interaction affinity with citrate. These findings play a key role for citrate functionalised AgNPs to be used as a low cost highly selective and sensitive lead ion sensor for potential application in industrial lead pollution monitoring. We have further varied several sensor parameters such as AgNPs size, concentration and the allowed reaction time for it to be practically implemented as an efficient lead sensor meeting the Environmental Protection Agency recommendations.

Keywords: Silver nanoparticles, Localized Surface Plasmon Resonance, Self-assembled nanoparticles, Aggregation, Theoretical modelling, Lead pollution

1. Introduction

Plasmonic nanomaterials being one of the emerging class of optically active nanomaterials not only appealing for basic studies, but have revolutionary application in several other fields including energy conversion, electronics, photonics, sensors and biomedical applications [1-3]. The plasmonic nature of metallic nanostructures exhibit a special property known as 'Localized Surface Plasmon Resonance' (LSPR) through the coherent electron oscillations in presence of photon incidence, which can bring the enhancement in the optical cross-sections, hot carrier generation, and so forth, at their surface [4]. The LSPR modes are known to be highly sensitive to the external dielectric environment of nanoparticles [5]. Modulation of LSPR band based on its sensitivity to the nearby medium has led to development of several nanosensors. Nanosensors based on nanoparticles (NPs) have proven to meet the age-old challenges in the field of chemical and biological sensing, as well as to tackle tremendous environmental pollution due to their highly sensitive and tuneable LSPR bands to its external environment [6]. Especially there are tremendous effort has been made in cleaning and monitoring of industrial as well as mining waste which contains high amount of various toxic and nonbiodegradable heavy metal pollutants (Hg, Cd, Zn, Ni, As, Pb etc.) [7,8]. Of these, our specific focus is on the detection of Pb^{2+} ions, which is one of the most toxic and worrisome pollutants. Lead is of particular interest, because of its toxicity and its widespread presence in the environment and appraised as a priority pollutant [9]. It is one of the devastating industrial pollutants, which enters the ecosystem through soil, air and water. Today the major exposures of lead into the environment are through human's action as mining, grinding and crushing of the ores, lead-based products such as lead-acid batteries [10], petrol additive, lead pipes and industrial wastage [11,12]. The industrial waste water contains upto 500 mg/L of Pb(II) which is very high compared to the Environmental Protection Agency (EPA) recommendations which is 0.05 mg/L [13]. So, it is highly desirable to detect lead from industrial waste-water before discharging into the environment.

Nanomaterials of noble metal such as Silver (Ag) and gold (Au) nanoparticles are the two most widely used plasmonic nano-markers with various surface modification to detect environment polluting heavy metals from different systems, possessing a high optical absorbance cross-section in UV-Visible region[14,15]. The presence of heavy metal ions in the system led to the self-aggregation or agglomeration of the NPs into different non-spherical geometry and clusters, driven by forces such as van der Waals interaction, ligand coupling, electrostatic attraction and repulsion between the charged particles etc [16-19]. As a result of it, size shape and physical environment of the NPs changes drastically, which lead to change in the shape of the LSPR band [20]. It is possible to detect these spectral changes using simple UV-Vis spectroscopy, or even in naked eyes as a crucial tool for

heavy metal ion detection [21,22]. Notably, silver NPs attract more attention over gold NPs due to its sensitivity, cost-effectiveness and higher molar extinction coefficient (100 times) which is advantageous when using for absorption spectroscopy [23,24]. Along with spectroscopy, several microscopy techniques such as electron and scanning microscopy have been regularly used for visualization and characterization of the formed NPs aggregates [25].

Although several silver nanoparticles-based studies have already been reported with different surface modifications based on Pb^{2+} interaction, however, investigation on the exact aggregation mechanism is still sparse in the literature [26-28]. Recently, some theoretical studies have been done in this direction which reveals that when two or more nanoparticles assemble new LSPR properties are observed [29-32]. Mei theory has been used extensively to understand the colloidal NPs systems and its complex aggregates. Although, we can emphasise the use of electrostatic models based on quasi-static approximation to deal with optical cross-section of NPs and their simpler aggregates. Keeping in mind the fact, we have done combined experimental and theoretical approach to establish the exact mechanism of interaction of Pb^{2+} with citrate functionalized silver NPs.

In this work, we have synthesized and characterized citrate functionalized silver nanoparticles (AgNPs) and done spectroscopic as well as analytical studies to understand the underlined aggregation mechanism after its interaction with Pb^{2+}. We have utilized the prominent changes in LSPR spectra of the AgNPs as a central sensing tool for Pb^{2+} detection, mostly due to the formation of one dimensional (1D) self-assembled chain-like geometry of NPs. The mechanism is based on the simultaneous quenching of the existing LSPR peak and generation of a new red shifted LSPR peak. For further details for the aggregation type, we have performed transmission electron microscopy (TEM) to visualize the corresponding geometrical changes and based on the findings of the TEM results we performed basic theoretical studies on nanoparticle and its aggregates. To establish the formation of self-assembled chain-like aggregated structures, fitting of the experimental data with analytically calculated optical cross-section equations have been done. Our study finds application in industrial Pb^{2+} monitoring for that we have varied several nanoparticle parameters for better sensitivity towards lower Pb^{2+} concentrations.

2. Materials and Methods

2.1. Materials

Trisodium citrate [$Na_3C_6H_5O_7$], silver nitrate [$AgNO_3$] and sodium borohydride [$NaBH_4$], were purchased from Sigma-Aldrich. All other metal precursors (in the form of chloride or nitrate) were purchased from either Sigma-

Aldrich or Merck. The chemicals, we have used were of analytical grade and all the solutions were prepared in Millipore water.

2.2. Synthesis of silver nanoparticles

Citrate functionalized silver nanoparticles (AgNPs) have been synthesized in aqueous solution by reduction method taking $NaBH_4$ as a reducing agent [33]. Briefly, 1 mL of 5mM $AgNO_3$ was added to 16 mL of 1 mM trisodium citrate under constant stirring in an ice/water bath at around 0° C, to this solution 100 µL of a freshly prepared 5 mM $NaBH_4$ over 5 minutes (min). The colourless solution gradually changed its colour upon the addition of the reducing agent and finally gained an intense yellow colour. This yellow-coloured colloidal solution was kept under stirring for 2 h at almost 0ºC. The as-prepared citrate functionalized silver NPs were stabilized for several weeks.

2.3. Characterization Methods

The optical absorbance characteristics were studied by Shimadzu UV-2600 spectrophotometer. All the measurements were taken in a quartz cuvette of optical pathlength equal to 1 cm with baseline corrected in water. The transmission electron microscopy (TEM) was used to visualize and characterize the detailed geometry and structure of the nanoparticles. The samples for the TEM studies were prepared by drop-casting the as-synthesized AgNPs and, Pb^{2+} added AgNPs on a carbon-coated copper mesh of 3 mm diameter [34]. The hydrodynamic diameter of the nanoparticles and their aggregates were measured by dynamic light scattering technique in Zetasizer Nano DLS instrument.

2.4. Procedure for Pb^{2+} induced sensing experiments:

All the UV-Visible (UV-Vis) absorbance spectra measurements of the AgNPs were carried out at room temperature. For Pb^{2+} measurement purposes, the required amount of as-prepared colloidal solution of the AgNPs (nanosensor) was added in the water maintaining the net volume equal to 2 mL. Stock solutions of varying concentrations of Pb^{2+} ions were prepared (suitable amount of lead nitrate $Pb(NO_3)_2$ was added to Millipore water to prepare the Pb^{2+} aqueous solution) and every time the same amount of the sensor was added into it. The temporal evolution of the plasmon resonance bands of AgNPs was also monitored and for this purpose, the mixture samples were stood for a definite time. The resultant self-assembled aggregates were visualized with the help of TEM.

2.5. Theoretical calculation of the absorption cross-section of self-assembled silver NPs and their aggregates:

The optical absorption cross-section was calculated by using the quasi-static response ($R \ll \lambda$, i.e. the particle size is much smaller than the wavelength of light) of a metal sphere in an electric field [35]. The interaction of light with these metal nanoparticles induces a dipole on the surface of the nanoparticles and thereafter the curved surface of the NP applies a restoring force on the free electron cloud (plasmon), resulting in their back-and-forth movement hence possess a natural frequency of oscillation. Our study is focused in the visible region of the electromagnetic spectrum since for silver, the natural frequency of dipole oscillation thereby the polarizability ($\alpha(\omega)$) concomitant a resonance enhancement in visible region and this resonance is named as 'Localized surface plasmon resonance'[14,36]. This resonance enhancement appears as an absorption peak [14] in UV-Vis absorbance spectroscopy. The optical absorption cross-section is directly proportional to the imaginary part of polarizability and given by the below equation as [37]:

$$\sigma_{abs} = \frac{K}{\varepsilon_0} \mathrm{Im}\,[\alpha(\omega)] \quad (1)$$

where K is the wave vector of incident light, ε_0 is vacuum permittivity and speed of light is taken 1. For an isolated metallic sphere of radius R in an external electric field of wavelength λ, the polarizability is given as [35]

$$\alpha(\omega) = 4\pi R^3 \varepsilon_0 \left(\frac{\varepsilon(\omega)-\varepsilon_m}{\varepsilon(\omega)+2\varepsilon_m}\right) \quad (2)$$

The dielectric constant (ε_m) of the medium i.e., aqueous colloidal silver nanoparticles solution was taken to be (1.768). We choose the dielectric function $\varepsilon(\omega)$ (frequency of electromagnetic radiation ω) which fits the experimental data given by Johnson and Christy for sliver in visible region [38]. The dielectric function of metals is complex and hence putting $\varepsilon(\omega)=\varepsilon_1+i\varepsilon_2$, solving for the imaginary part we have of polarizability

$$\mathrm{Im}[\alpha] = \frac{3\varepsilon_m\varepsilon_2}{(\varepsilon_1+2\varepsilon_m)^2+{\varepsilon_2}^2} \quad (3)$$

Putting this value in equation (1)

$$\sigma_{abs(1)} = \frac{8\pi^2 R^3}{\lambda}\left(\frac{3\varepsilon_m\varepsilon_2}{(\varepsilon_1+2\varepsilon_m)^2+{\varepsilon_2}^2}\right) \quad (4)$$

Where, ε_1 and ε_2 separately follows the experimental values given by Johnson and Christy. After interaction with Pb^{2+} ions, NPs were aggregated mostly to form chain-like structures made of various numbers of NP. The sizes

of the formed nanoparticle aggregates were assumed to be small concerning the wavelength of incident light (λ) such that quasi-static approximation remains valid. If two or more nanoparticle comes closer to each other in such a way that there is a significant overlapping of their dipolar electromagnetic fields, the localized plasmon resonance of individual particles couple to each other to give new resonance modes [16,35]. The resultant polarizability for two in-phase modes of the nanoparticle-pair system was taken using the assumption that the two particles have the same radius (R) and given by the following equation [35],

$$\alpha(\omega) = 4\pi R^3 \varepsilon_0 \frac{\eta}{3}\left(\frac{1}{1-2\eta\left(\frac{R}{D}\right)^3} + \frac{2}{1+\eta\left(\frac{R}{D}\right)^3}\right) \quad (5)$$

Where, $\eta = \left(\frac{\varepsilon(\omega)-\varepsilon_m}{\varepsilon(\omega)+2\varepsilon_m}\right)$ and D is the centre to centre distance of the two particles. Solving for the imaginary part of equation (5), we got the absorption cross-section for the pair system as,

$$\sigma_{abs}(2) = \frac{8\pi^2 R^3}{\lambda}\left\{\frac{1}{3}\left(\frac{\varepsilon_m \varepsilon_2 (2m+l)}{(\varepsilon_1 l+2\varepsilon_m m)^2+\varepsilon_2{}^2 l^2}\right) + \frac{2}{3}\left(\frac{\varepsilon_2 \varepsilon_m (n+o)}{(\varepsilon_1 n+\varepsilon_m o)^2+\varepsilon_2{}^2 n^2}\right)\right\} \quad (6)$$

Where $m = 1 + \left(\frac{R}{D}\right)^3$, $l = 1 - 2\left(\frac{R}{D}\right)^3$, $n = 1 + \left(\frac{R}{D}\right)^3$ $o = 2 - \left(\frac{R}{D}\right)^3$. Here, we have taken D = 2R for calculation purposes. $\sigma_{abs}(1), \sigma_{abs}(2)$ represent the absorption cross-section equations for single NP and NP-pair system respectively and would be used to develop model equations for the fitting of the observed experimental LSPR band. To fit the experimentally obtained absorbance peaks, the obtained absorption cross-section equations were first normalized by their magnitude at found LSPR peak values.

3. Result and Discussion

3.1. Characterization of AgNPs

The as-prepared citrate functionalized silver nanoparticle's (AgNPs) aqueous colloidal solution has been characterized by UV-Vis spectrophotometry. The UV-Vis absorbance spectra of the AgNPs in increasing order of concentration of nanosensor shown in Fig. 1 (a) indicate that the optical density (O.D.) increases with an increase in the concentration of the NPs. Inset of Fig. 1 (a) shows the pictorial image of yellow coloured colloidal AgNPs solution. The characteristic LSPR absorbance band of AgNP is found to be peaking at around 395 nm which is consistent with previously reported literature for citrate functionalized silver nanoparticles [39]. Dynamic light scattering has been performed for an idea of average hydrodynamic diameter of the AgNPs. Fig. 1 (b) shows the volume distribution of hydrodynamic diameter of the AgNPs having an average hydrodynamic diameter equal

to 15 nm. The exact size distribution and characterization of the AgNPs have been done using TEM imaging method. From the TEM image of AgNPs shown in Fig. 1 (c), we confirm the almost spherical shape and uniform size distribution of the NPs. The average diameter of the AgNP has been calculated and is found ~8 nm (upper inset of Fig. 1 (c)). The high-resolution transmission electron microscope (HRTEM) image analysis of NP (lower inset of Fig. 1 (c)) demonstrates the crystalline nature of the metal AgNPs owing to uni-directional lattice growth with a fringe spacing of around 0.23 nm which is consistent with the reported fringe distance of Ag [111] plane [40,21]. The LSPR peak of prepared AgNPs is found to be around 395 nm and is due to the presence of non-aggregated single NPs which has been used for further studies. We have now studied the aggregation of AgNPs in presence of Pb^{2+} ions by analysing the LSPR spectra of AgNPs in presence of Pb^{2+}.

3.2. Pb^{2+} interaction and possible interaction mechanism

In presence of Pb^{2+} ions, AgNPs have started to form non-spherical aggregates. The interaction mechanism is governed by the physiochemical changes in terms of arisen of new LSPR bands of AgNPs due to the formation of aggregated structure upon interaction with Pb^{2+}. A new absorption band at ~470-520 nm (Fig. 2 (a)) along with the existing one is found to be observed after the addition of Pb^{2+} in the AgNPs solution. At the same time, the intensity of the LSPR peak at ~395 nm reduces as an effect of Pb^{2+} addition. The simultaneous existence of two peaks can be attributed to the presence of Pb^{2+} in the system. The appearance of a new red-shifted peak at around 470-520 nm is due to the formation of larger self-assembled aggregates of AgNPs. It is observed from Fig. 2 (a) that the band centre at around 470-520 nm undergoes a gradual red shift and concurrently the O.D. of the peak also increases with the increment of Pb^{2+} ion. The appearance of two LSPR peaks at 395 nm (denoted as peak 1) and around 470-520 (denoted as peak 2) nm is due to the non-spherical arrangement of the NPs. Overall, these spectroscopic findings indicating that the formed aggregated geometry is similar to that of due to self-assembly of NPs into one-dimensional linear chains [29]. Here, the two peaks can be ascribed to the existence of two simultaneous modes, one longitudinal and another transverse, which is associated with the surface plasmon oscillation of electron cloud along and perpendicular to the axis of one-dimensional self-assembled chain like architecture of the NPs [41]. With variation in chain length the charge distribution along the longitudinal axis, consequently, the resonance condition varies and hence the corresponding absorption peak. The observed gradual red shift of peak 2 upon gradual increment in lead concentration can be hypothesized due to the growth in chain length. Inspired from this spectroscopic result we performed DLS and TEM measurements to know the exact aggregate type. It is evident from Fig. 2 (b) that the average hydrodynamic diameter of the system (calculated

using DLS) increases with the increment on Pb^{2+} in the system which is an indication of formation of larger aggregates. TEM analysis has proven to be a more confirmatory tool for the hypothesis of self-assembled chain like geometry of AgNPs. TEM image of the Pb^{2+} added AgNPs system shown in Fig. 2 (c) reveal that due to the presence of Pb^{2+}, AgNPs come closer to each other forming NPs chains such that Pb^{2+} matrix would have acted to couple the AgNPs together. It is also apparent from HRTEM images shown in Fig. 2 (d, e) that the formed NP chain aggregates are made of various length. However, it is observed that some of the NPs remain intact (i.e. do not form aggregates). The increment of peak 2 and decrement of peak 1 upon lead (Pb) addition indicates a diminishing number of free nanoparticles with the concurrent increase in a number of self-assembled NPs. Further, to understand the compositional analysis of lead added AgNPs system, we have performed Energy-filtered transmission electron microscopy (EFTEM). It can be elucidated from the EFTEM map shown in Fig. 2 (g, h) that NP-assemblies are embedded by the lead matrix. The mechanism could be explained such as the charged NPs might have come closer to each other via electrostatic attraction with the oppositely charged divalent lead ions in such a way that it surrounds the nearby matrix of the chain like geometry of NPs. It is also noticeable that lead has a high interaction affinity with citrate [42]. The citrates molecules which are adsorbed on the AgNPs surface contains free carboxylate group (Park et al, 2014, reported this for AuNPs) [43] and therefore are favourable for interaction with Pb^{2+}.

3.3. Theoretical modelling of self-assembled silver NPs chains after interaction with Pb^{2+}

Throughout this discussion, UV-vis and TEM result both supports the argument that in presence of Pb^{2+} NPs form 1D chain like geometry which is responsible for the generation of new LSPR mode along with the existing one. Here, by the help of basic theoretical understanding, we developed some analytical equations based nanoparticles and nanoparticle aggregates which is going to boost our experimental results. In this current work, the plasmon absorption cross-section of single nanoparticles and nanoparticle pair cluster systems have been calculated analytically using the basic electrostatic results in the quasi-static regime. Metals possess a complex dielectric function and, therefore, the real and imaginary parts of the dielectric function have been separately calculated based on the experimental finding of Johnson and Christy for silver (Ag) [38].

$$\varepsilon_1 = A_1 \exp(-A_2\lambda) + A_3 \tag{7}$$

$$\varepsilon_2 = 2C_1 \left\{ B_1 + \left(\frac{B_2\lambda^2}{{B_3}^2+\lambda^2} \right) \right\} \tag{8}$$

The equations (7), (8) follows the fitted curve respectively for the real and imaginary part of dielectric function with the appropriate real valued constants A_1, A_2, A_3, B_1, B_2, B_3, C_1. The wavelength dependency of the absorption cross-section equations has incorporated through the expressions of dielectric constant. The growth of NPs to NP chains and their corresponding plasmon evaluation have been well understood by the fitting of the experimentally obtained results with absorption cross-section equations of appropriate NPs geometries. To explain the effect of Pb^{2+} on AgNPs aggregation and plasmon modification, the absorption cross-section equations and, the resonance conditions have been investigated both before and after the addition of Pb^{2+}. The LSPR spectra of the AgNPs before and after the addition of Pb^{2+} are shown in Fig. 3 (a) and are named as spectrum 1 (without Pb^{2+}), spectrum 2 (16 ppm Pb^{2+}), spectrum 3 (23 ppm Pb^{2+}). The resonance enhancement condition for single NP systems (i.e. when $\varepsilon_1=-2\varepsilon_m$) satisfied by equation (4), for a particle of 10 nm diameter, is found to be near 395 nm which is equal to the experimentally observed spectral peak of the AgNPs. Hence, this theoretically obtained absorbance cross-section expression of a single NP normalized at 395 nm taking wavelength of incident light (λ) to be an independent variable has found to best fit the observed normalized LSPR spectrum 1 (shown in Fig. 3(b)). Earlier in our discussion, we have predicted that AgNPs form 1D chain like geometry in presence of Pb^{2+}. It is appropriate now to discuss the absorption cross-section calculations for NP aggregates especially the 1D chains. Here, we have limited our discussion to the NP pair systems. The absorption cross-section for a NP pair system has been calculated by the previously mentioned procedure and given by equation (6). The resonance enhancement in this case (particles of diameter 10 nm) has been found to get satisfied twice giving two in-phase modes, one transverse mode (~395 nm) which is perpendicular to the electric field and the other longitudinal mode (~470 nm, along the chain axis) which is parallel to the field, however, there also exist two opposite phase modes but, only the in-phase modes are dominant for optical excitation when considering for quasi-static approximation i.e. for small NPs [35]. As we investigated earlier not all NPs form aggregates upon interaction with lead, the normalized LSPR spectrum 2 and spectrum 3 have been fitted by taking contribution from both i.e., single NP (equation (4)) and NP pair system (equation (6)) depending on the lead ion concentration. With an increment in lead concentration the tendency of NPs to form longer aggregates increases and therefore we have taken a higher contribution from NP pair system for spectrum 3 compared spectrum 2 for fitting purpose. The equations which have been found to be the best fit the normalized spectrum 2 and spectrum 3 are given by equations (9) and (10) as follows:

$$\sigma_{abs} = \frac{8\pi^2 R^3}{\lambda}\{5(\sigma_{abs}(1)) + 2(\sigma_{abs}(2))\} \quad (9)$$

$$\sigma_{abs} = \frac{8\pi^2 R^3}{\lambda}\{5(\sigma_{abs}(1)) + 9(\sigma_{abs}(2))\} \quad (10)$$

It is evident from both the equations that the contribution of single NPs to NP pairs has increased from 5:2 to 5:9 as lead concentration increased. The fitted curves along with their experimentally observed normalized absorption spectra are shown in Fig. 3 (c), 3 (d) and found to be in good agreement with each other. The fitting parameters, appeared via ε_1 and ε_2, for the three spectra namely 1,2,3 have tabulated in Table 1. The spectroscopic results for much higher Pb^{2+} concentrations as observed (Fig. 2 (a)) are also in accordant with many previously reported theoretical studies that have been done for silver nanoparticle linear chains. These studies confirm the fact that the absorbance corresponding to longitudinal mode undergoes a red shift when more NPs couple to form longer chains [44,35]. It justifies and supports our interpretation that with increment in Pb^{2+} concentration more AgNPs assembled to form longer chains which lead to much red shifted LSPR peaks.

3.4. Optimization of various parameters of AgNPs to be as an efficient Lead sensor:

Although we have established mechanism of the change of plasmonic properties in AgNPs in presence of Pb^{2+} ion, it is highly desirable to utilize this fact for practical application purpose. Lead is heavily toxic and priority pollutant [12]. One of the main sources of lead pollution is from industrial waste-water which contains a very high concentration upto 500 mg/L of Pb^{2+} [13]. So, it is very important to detect Pb^{2+} ion from industry waste-water. The direct resemblance of variation in AgNPs LSPR spectra with Pb^{2+} concentration can be very beneficial when utilized as a lead detecting nanosensor. There are many parameters which affect the interaction affinity of the AgNPs towards the Pb^{2+}. Of them, particle size, nanoparticle concentration and probing time plays a very crucial role in order to increase the limit of detection (LOD) of the AgNP sensor [45]. In the present section, we have systematically varied different parameter to improve the LOD of the nanosensor for Pb^{2+} detection.

Size dependency:

As the LSPR band highly depends on the size of the NP, it is expected that smaller size AgNPs have a higher affinity towards heavy metal ions than larger ones due to their higher surface to volume ratio [46]. The synthesis procedure of silver NPs plays a critical role in the production of smaller and monodispersed silver NPs, which affects the aggregation response very much. We have synthesized two sets of AgNPs namely NPs_1 and NPs_2 having an average hydrodynamic diameter equal to 40 nm and 15 nm respectively. The UV-Vis absorbance spectra as shown in Fig. 4 (a), clearly delineate that NPs_1 have broadened LSPR band than NPs_2 due to its larger and nonuniform size distribution. The sensitivity of both the NPs (at the same concentration) towards Pb^{2+} has been observed. It is noticed from Fig. 4 (b), 4 (c) that, in case of NPs_2 a dominant LSPR band has been generated at

~500 nm whereas for same lead concentration there is no such significant band appeared with NPs_1. From this observation, we can conclude that the probability of AgNPs to couple to form NP chains is much higher in smaller sized NPs (15 nm) than larger one (40 nm) hence shows higher response with NPs_2. Thereby we have used NPs_2 now onwards for further parameter dependency investigations.

Concentration dependency:

The concentration of nanoparticle in the solution plays another pivotal role to increase lead ion interaction sensitivity in terms of LSPR modes. The accurate estimation of the AgNPs concentration is quite difficult to calculate since each batch of NPs varies in size and shape. However, we need to have an approximate idea of the AgNPs concentration which have been calculated using previously reported theoretical results taking the molar extinction coefficient of citrate capped silver nanoparticle of diameter 10 nm equal to 5.56×10^8 M^{-1} cm^{-1} [47]. The molar concentration of the AgNPs has been calculated using Beer-Lambert law. Here, we have taken three different concentrations (in increasing order) of NPs_2 and investigated the effect of concentration on interaction affinity. Fig. 4 (d, e & f) illustrate the UV-Vis spectral response of three different concentrations i.e. 0.4 a.u (~700 μM), 0.2 a.u. (~360 μM) and 0.1 a.u (~180 μM) of AgNPs sensor respectively in presence of same lead ions. It is found that spectral changes increase with the decrement of sensor concentration. Hence, for prepared AgNPs to be used as a lead sensor we must need to use minimal possible AgNPs concentration for better sensitivity. It may be due to fact that the contribution from the excess unreacted AgNPs subdue the contribution from aggregated ones.

Temporal dependency:

We have also investigated how the interaction affinity of AgNPs towards Pb^{2+} detection changes with respect to time. Significant spectral changes have been noticed up to 60 minutes of incubation time. The temporal variation of the AgNPs for 0 to 25 ppm of Pb^{2+} shown in Fig. 5, where 0 ppm is the control spectral response of the AgNPs without lead. It is observed that, the LSPR peak height of AgNPs decreases with time, additionally second peak (~500 nm) height increases simultaneously. This result suggests that the interaction affinity of AgNPs increases with longer incubation time. Moreover, there is a significant red shift of the second peak with respect to time for all cases. Here, 60 min of reaction time could be considered as enough for Pb^{2+} detection, beyond which insignificant changes have been observed. The sensitivity of AgNPs increases with higher incubation time. To get insights of the nature of sensor response towards Pb^{2+} the relative difference of the two absorption peak heights

(I_0-I) before and upon interaction with varying Pb^{2+} concentration has been plotted and shown in Fig. 6 (a, b). I_0 is the absorbance of the AgNPs before interaction with Pb^{2+} at peak positions 395 and 520 nm whereas I represent the absorbance measured after 60 min of incubation with Pb^{2+} at same peak positions. Fig. 6(a) demonstrates the differential absorbance (I_0-I) for all concentrations from 0 ppm- 25 ppm at 395 nm which follows non-linearity given by equation $Y = 0.08 - 0.09\exp(-X/16.04)$, where Y is the differential absorbance and X represent the Pb^{2+} ion concentration. However, the region between 0 ppm-10 ppm exhibits a good linear correlation (correlation coefficient (r^2) = 0.98) and shown in the inset of Fig. 6 (a). Similarly, at 520 nm there is a complete linear response of the sensor with Pb^{2+} having a correlation coefficient equal to 0.98 (Fig. 6 (b)). Here, 60 min of reaction time could be considered as enough for Pb^{2+} detection, beyond which insignificant changes have been observed. The limit of detection is ~1.5 ppm, which has been obtained from the linear region (0 -10 ppm) corresponding to peak 1 [48]. Thus, the present discussion demonstrates that by varying the size, concentrations of AgNPs and allowing for enough reaction time, better sensitivity has been achieved.

3.5. Interaction affinity of AgNPs sensor towards other heavy metal ions:

Further, we have checked out the LSPR response of AgNPs with various other metal ions present in the environment. We have investigated the spectral response AgNPs towards other relevant metal ions such as Hg^{2+}, Ni^{2+}, Fe^{3+}, Ca^{2+}, Co^{2+}, Cu^{2+}, Cd^{2+}, Mg^{2+}, As^{3+}, K^{+}, Na^{+} under the same experimental conditions. The study shows (Fig. 7) that other than Pb^{2+} above-mentioned metal ions do not show any significant spectral changes upon interaction with the prepared AgNPs (spectra not shown). Although, for Hg^{2+} a blue shift is observed in the LSPR spectra of AgNPs however it is followed completely different aggregation/agglomeration mechanism since no new LSPR modes have observed. Hence our citrate-based silver NPs proved to be highly selective Pb^{2+} sensor.

4. Conclusion

In summary, we have investigated the role of Pb^{2+} towards definite one-dimensional chain like self-aggregation of citrate capped silver nanoparticle using UV-visible, DLS and TEM measurement supported with analytically calculated absorption cross-section equations for NPs and NP-pair system based on quasi-static approximation. Self-assembled anisotropic geometry of formed 1D NPs chain leads to the coupling nearby LSPR modes of NPs thereby new modes at a higher wavelength (~520 nm) have generated along with existing LSPR band (~395 nm). TEM and HRTEM images of the lead added AgNPs systems confirms the formation of 1D self-assembled geometry of NPs. The fact that increment in Pb^{2+} concentration leads to the formation of longer NP chains is

verified by the fitting of analytically calculated NP and NP-pair equations in an appropriate ratio. Eventually we optimize several other NP parameters such as size, concentration and interaction time towards AgNPs to be utilized as an efficient Pb^{2+} sensor. It is observed that smaller sized NPs (~8 nm) with minimal AgNPs concentration (O.D. ~ 0.1) when allowed for 60 min of interaction time gives better response even in presence of low Pb^{2+} concentration (~3 ppm). Presence of other relevant metal ions is also been studied which suggests that only Pb^{2+} is capable of generation of 1D chain like geometry of the NPs. Overall, this study gives incites to the detailed 1D self-assembly of AgNPs in presence of Pb^{2+} and AgNPs has been proven to be used as a highly selective, favourably sensitive tool to detect lead for potential application in industrial wastewater pollution monitoring.

Declarations

Author contribution: N.P. performed the synthesis, optical characterization and sensing experiments, analysed the data, prepared all figures and contributed to writing the manuscript. T.K.M. assisted in performing the experiments, contributed in scientific discussion and helped in writing the manuscript. S.B., N.P. and Arpita C. performed the theoretical modelling and the analytical calculations. Arka C. and P.B. assisted in performing and analysing sensing experiment, and contributed in scientific discussion, and manuscript revision. M.M. and Arpita C, assisted in providing research plan, and contributed to the scientific discussion. S.K.P. provided the research plan, assisted in scientific discussion and wrote the manuscript. All authors reviewed the manuscript**.**

Funding: We thank Abdul Kalam Technology Innovation National Fellowship (INAE/121/AKF) for funding.

Conflicts of interest: The authors declare there is no conflict of interest.

Availability of data and material: All data generated or analysed during this study are included in this article.

Code availability: Not applicable.

Ethics approval: Not applicable.

Consent to participate: Not Applicable.

Consent for publication: Not applicable.

References

1. Jain PK, Huang X, El-Sayed IH, El-Sayed MA (2007) Review of some interesting surface plasmon resonance-enhanced properties of noble metal nanoparticles and their applications to biosystems. Plasmonics 2 (3):107-118
2. Wu N (2018) Plasmonic metal–semiconductor photocatalysts and photoelectrochemical cells: a review. Nanoscale 10 (6):2679-2696
3. O'Connor D, Zayats AV (2010) The third plasmonic revolution. Nat Nanotech 5 (7):482-483
4. Gray SK (2007) Surface plasmon-enhanced spectroscopy and photochemistry. Plasmonics 2 (3):143-146
5. Kelly KL, Coronado E, Zhao LL, Schatz GC (2003) The optical properties of metal nanoparticles: the influence of size, shape, and dielectric environment. ACS Publications,
6. Homola J, Piliarik M (2006) Surface plasmon resonance (SPR) sensors. In: Surface plasmon resonance based sensors. Springer, pp 45-67
7. Knecht MR, Sethi M (2009) Bio-inspired colorimetric detection of Hg 2+ and Pb 2+ heavy metal ions using Au nanoparticles. Anal Bioanal Chem 394 (1):33-46
8. Wu Y, Pang H, Liu Y, Wang X, Yu S, Fu D, Chen J, Wang X (2019) Environmental remediation of heavy metal ions by novel-nanomaterials: a review. Environ Pollut 246:608-620
9. Gao B, Chi L, Mahbub R, Bian X, Tu P, Ru H, Lu K (2017) Multi-omics reveals that lead exposure disturbs gut microbiome development, key metabolites, and metabolic pathways. Chem Res Toxicol 30 (4):996-1005
10. Bode H (1977) Lead-acid batteries.
11. Gupta VK, Ali I (2004) Removal of lead and chromium from wastewater using bagasse fly ash—a sugar industry waste. J Colloid Interface Sci 271 (2):321-328
12. Harrison RM, Laxen D (1981) Lead pollution. In: Causes and Control. Springer,
13. Arbabi M, Hemati S, Amiri M (2015) Removal of lead ions from industrial wastewater: A review of Removal methods. Int J Epidemiol Res 2 (2):105-109
14. Maier SA (2007) Plasmonics: fundamentals and applications. Springer Science & Business Media,
15. Khurana K, Jaggi N (2021) Localized Surface Plasmonic Properties of Au and Ag Nanoparticles for Sensors: a Review. Plasmonics. doi:10.1007/s11468-021-01381-1
16. Zhang H, Fung K-H, Hartmann Jr, Chan CT, Wang D (2008) Controlled chainlike agglomeration of charged gold nanoparticles via a deliberate interaction balance. J Phys Chem C 112 (43):16830-16839
17. Zhang H, Wang D (2008) Controlling the growth of charged-nanoparticle chains through interparticle electrostatic repulsion. Angew Chem 120 (21):4048-4051
18. Lin Y-W, Huang C-C, Chang H-T (2011) Gold nanoparticle probes for the detection of mercury, lead and copper ions. Analyst 136 (5):863-871
19. Vilela D, González MC, Escarpa A (2012) Sensing colorimetric approaches based on gold and silver nanoparticles aggregation: chemical creativity behind the assay. A review. Anal Chim Acta 751:24-43
20. Guo M, Law W-C, Liu X, Cai H, Liu L, Swihart MT, Zhang X, Prasad PN (2014) Plasmonic semiconductor nanocrystals as chemical sensors: Pb 2+ quantitation via aggregation-induced plasmon resonance shift. Plasmonics 9 (4):893-898
21. Sarkar PK, Halder A, Polley N, Pal SK (2017) Development of highly selective and efficient prototype sensor for potential application in environmental mercury pollution monitoring. Water Air Soil Pollut 228 (8):314
22. Alizadeh A, Khodaei M, Karami C, Workentin M, Shamsipur M, Sadeghi M (2010) Rapid and selective lead (II) colorimetric sensor based on azacrown ether-functionalized gold nanoparticles. Nanotechnology 21 (31):315503
23. Thompson DG, Enright A, Faulds K, Smith WE, Graham D (2008) Ultrasensitive DNA detection using oligonucleotide− silver nanoparticle conjugates. Anal Chem 80 (8):2805-2810
24. Sarkar PK, Polley N, Chakrabarti S, Lemmens P, Pal SK (2016) Nanosurface energy transfer based highly selective and ultrasensitive “turn on” fluorescence mercury sensor. ACS Sens 1 (6):789-797
25. Di Stasio S (2001) Electron microscopy evidence of aggregation under three different size scales for soot nanoparticles in flame. Carbon 39 (1):109-118
26. Qi L, Shang Y, Wu F (2012) Colorimetric detection of lead (II) based on silver nanoparticles capped with iminodiacetic acid. Microchim Acta 178 (1-2):221-227
27. Cao H, Wei M, Chen Z, Huang Y (2013) Dithiocarbamate-capped silver nanoparticles as a resonance light scattering probe for simultaneous detection of lead (II) ions and cysteine. Analyst 138 (8):2420-2426
28. Tagar ZA, Memon N, Agheem MH, Junejo Y, Hassan SS, Kalwar NH, Khattak MI (2011) Selective, simple and economical lead sensor based on ibuprofen derived silver nanoparticles. Sens Actuators B Chem 157 (2):430-437
29. Xi C, Marina PF, Xia H, Wang D (2015) Directed self-assembly of gold nanoparticles into plasmonic chains. Soft Matter 11 (23):4562-4571

30. Hao E, Schatz GC (2004) Electromagnetic fields around silver nanoparticles and dimers. J Chem Phys 120 (1):357-366
31. Zuloaga J, Prodan E, Nordlander P (2009) Quantum description of the plasmon resonances of a nanoparticle dimer. Nano Lett 9 (2):887-891
32. Szalai A, Sipos Á, Csapó E, Tóth L, Csete M, Dékány I (2013) Comparative study of plasmonic properties of cysteine-functionalized gold and silver nanoparticle aggregates. Plasmonics 8 (1):53-62
33. Flores C, Diaz C, Rubert A, Benítez G, Moreno M, de Mele MFL, Salvarezza R, Schilardi P, Vericat C (2010) Spontaneous adsorption of silver nanoparticles on Ti/TiO2 surfaces. Antibacterial effect on Pseudomonas aeruginosa. J Colloid Interface Sci 350 (2):402-408
34. Maji TK, Hasan MN, Ghosh S, Wulferding D, Bhattacharya C, Lemmens P, Karmakar D, Pal SK (2020) Development of a magnetic nanohybrid for multifunctional application: From immobile photocatalysis to efficient photoelectrochemical water splitting: A combined experimental and computational study. JPhotochem Photobiol A: Chem:112575
35. Kreibig U, Vollmer M (1995) Theoretical considerations. In: Optical properties of metal clusters. Springer, pp 13-201
36. Hutter E, Fendler JH (2004) Exploitation of localized surface plasmon resonance. Adv Mater 16 (19):1685-1706
37. Kreibig U (1986) Optical properties of small particles in insulating matrices. In: Contribution of Clusters Physics to Materials Science and Technology. Springer, pp 373-423
38. Johnson PB, Christy R-W (1972) Optical constants of the noble metals. Phys Rev B 6 (12):4370
39. Maji TK, Bagchi D, Pan N, Sayqal A, Morad M, Ahmed SA, Karmakar D, Pal SK (2020) A combined spectroscopic and ab initio study of the transmetalation of a polyphenol as a potential purification strategy for food additives. RSC Adv 10 (10):5636-5647
40. Rodríguez-León E, Iñiguez-Palomares R, Navarro RE, Herrera-Urbina R, Tánori J, Iñiguez-Palomares C, Maldonado A (2013) Synthesis of silver nanoparticles using reducing agents obtained from natural sources (Rumex hymenosepalus extracts). Nanoscale Res Lett 8 (1):318
41. Xia H, Su G, Wang D (2013) Size-Dependent Electrostatic Chain Growth of pH-Sensitive Hairy Nanoparticles. Angew Chem 125 (13):3814-3818
42. Kourgiantakis M, Matzapetakis M, Raptopoulou C, Terzis A, Salifoglou A (2000) Lead–citrate chemistry. Synthesis, spectroscopic and structural studies of a novel lead (II)–citrate aqueous complex. Inorganica Chim Acta 297 (1-2):134-138
43. Park J-W, Shumaker-Parry JS (2014) Structural study of citrate layers on gold nanoparticles: role of intermolecular interactions in stabilizing nanoparticles. J Am Chem Soc 136 (5):1907-1921
44. Pellegrini G, Mattei G, Bello V, Mazzoldi P (2007) Interacting metal nanoparticles: Optical properties from nanoparticle dimers to core-satellite systems. MAT SCI ENG C-MATER 27 (5-8):1347-1350
45. Caucheteur C, Guo T, Albert J (2015) Review of plasmonic fiber optic biochemical sensors: improving the limit of detection. Anal Bioanal Chem 407 (14):3883-3897
46. Mehrdel B, Othman N, Aziz AA, Khaniabadi PM, Jameel MS, Dheyab MA, Amiri I (2020) Identifying Metal Nanoparticle Size Effect on Sensing Common Human Plasma Protein by Counting the Sensitivity of Optical Absorption Spectra Damping. Plasmonics 15 (1):123-133
47. Paramelle D, Sadovoy A, Gorelik S, Free P, Hobley J, Fernig DG (2014) A rapid method to estimate the concentration of citrate capped silver nanoparticles from UV-visible light spectra. Analyst 139 (19):4855-4861
48. Khadro B, Sanglar C, Bonhomme A, Errachid A, Jaffrezic-Renault N (2010) Molecularly imprinted polymers (MIP) based electrochemical sensor for detection of urea and creatinine. Procedia Eng 5:371-374

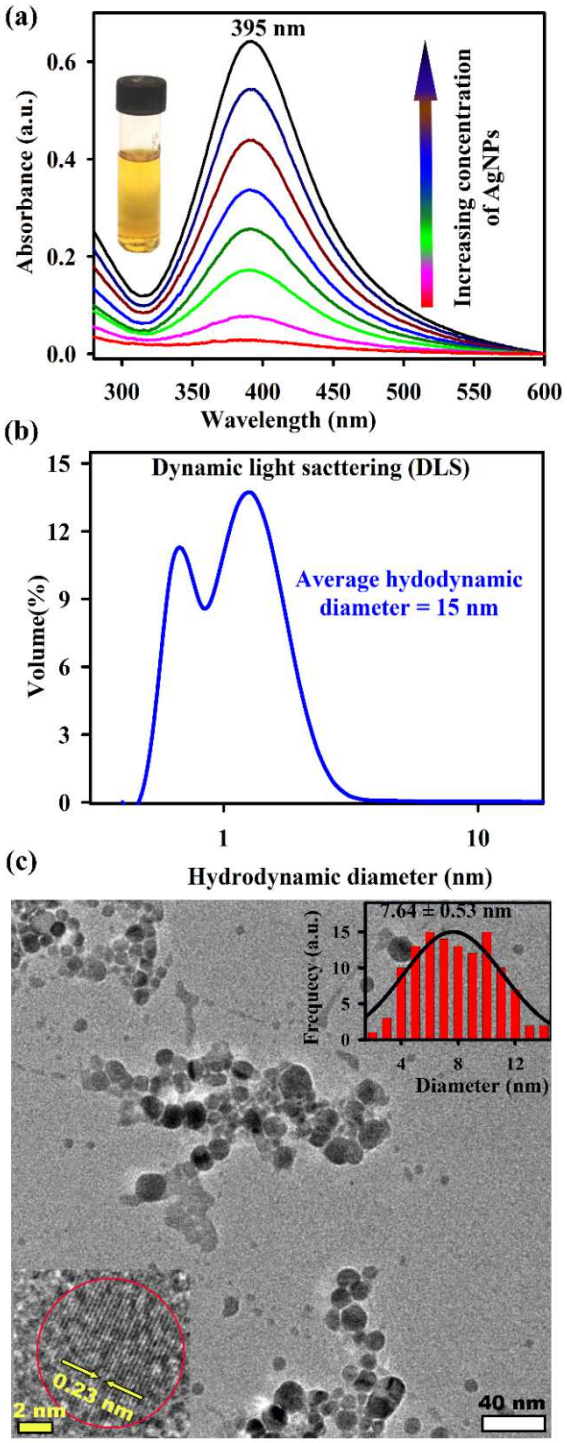

Fig. 1 (a) UV–Vis absorbance spectra of citrate capped silver nanoparticle's (AgNPs) colloidal solution with varying concentration of AgNPs. The Inset shows the image of the colloidal solution. **(b)** Volume distribution of hydrodynamic diameter (axis in common logarithm) of AgNPs measured using Dynamic Light Scattering. **(c)** TEM image of the AgNPs. Upper inset shows the size distribution of the AgNPs and lower inset shows a HRTEM image of the NP.

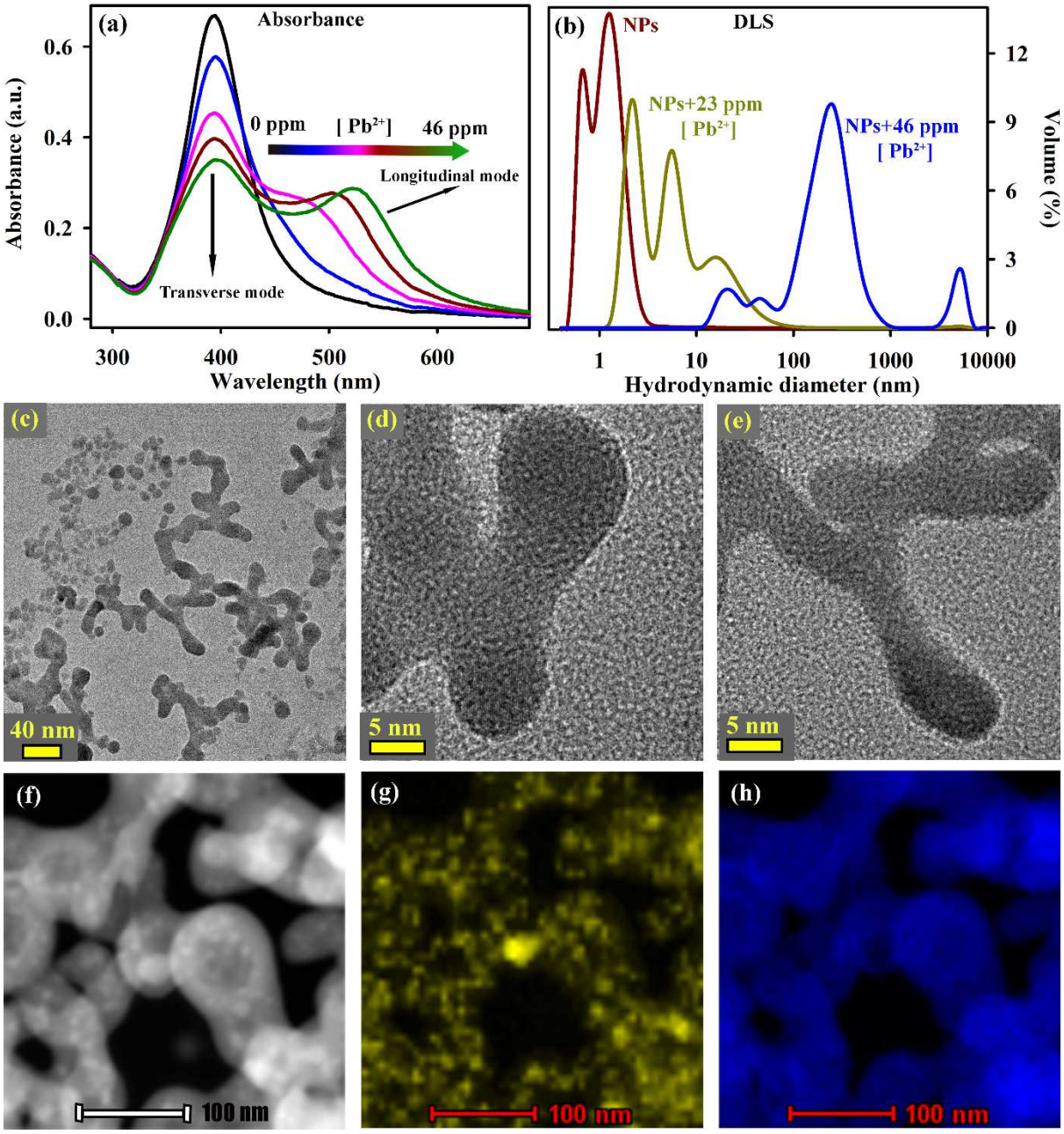

Fig. 2 (a) UV-Vis absorbance spectra of AgNPs after interaction with Pb^{2+} in increasing order of concentration of Pb^{2+}. **(b)** Volume distribution of hydrodynamic diameter of AgNPs (in Black) before and after interaction with two different concentrations of Pb^{2+} (in Green 23 ppm and Blue 46 ppm). **(c)** TEM image of the AgNPs after interaction with Pb^{2+}. **(d, e)** HRTEM images the AgNPs after the interaction with Pb^{2+}, showing chain like geometry of the NPs of varying chain length. **(f)** Drift corrected spectrum image scanning display of lead added NP aggregates and its EFTEM compositional analysis are shown in panel (g, h). **(g, h)** Yellow and Blue represents the presence of silver and lead respectively.

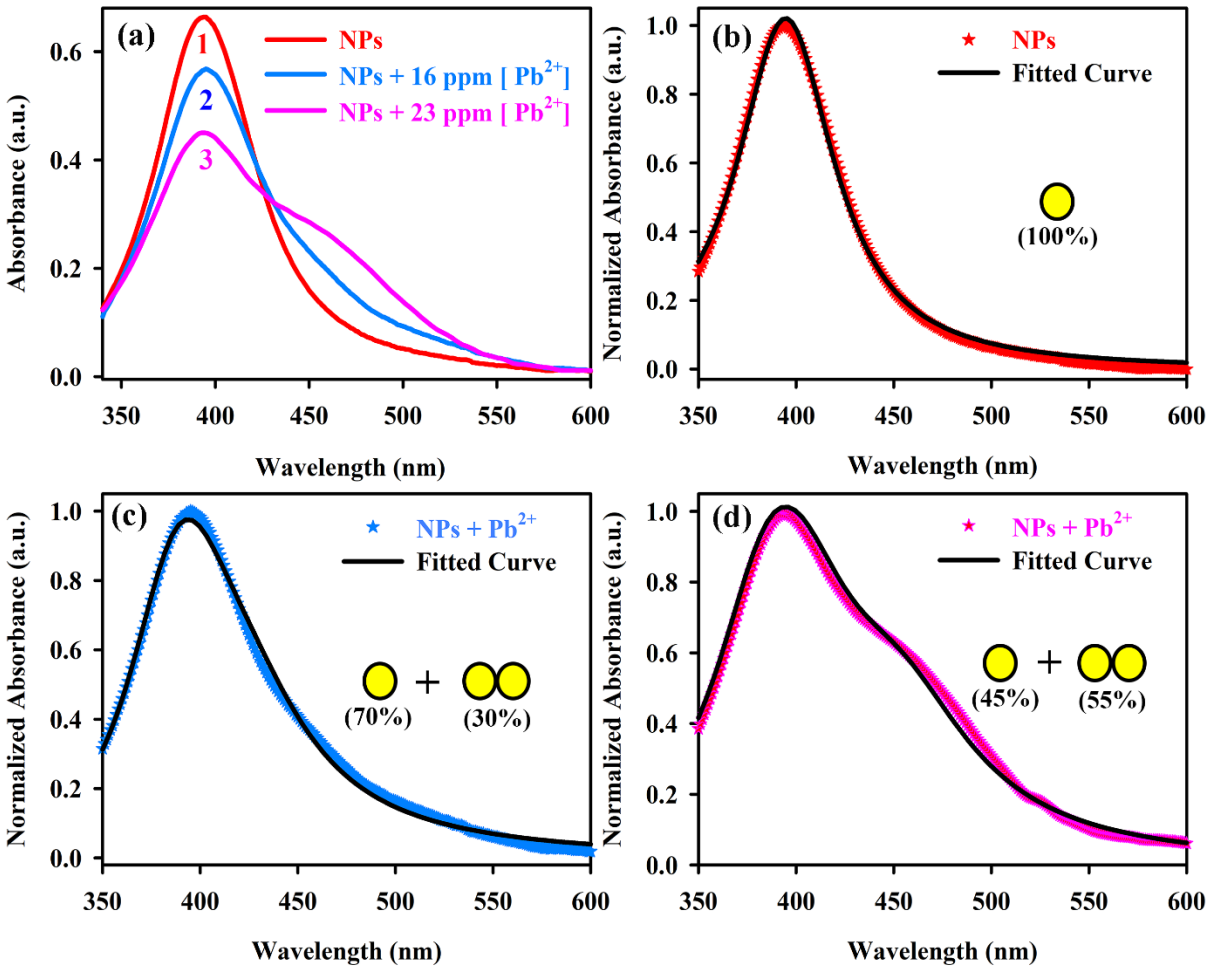

Fig. 3 (a) UV-Vis absorbance spectra of AgNPs before (red) and after interaction with 16 ppm (Blue), 23 ppm (Pink) of Pb^{2+}. The normalized UV-Vis absorbance spectra (as numbered in (a)) and the fitted curve (in Black) based on their corresponding equation for absorption cross-section equations are represented in panels from (b-d). The normalized UV-Vis absorbance spectra of **(b)** AgNPs before interaction with Pb^{2+} and its fitted curve following equation (4) for absorption cross-section of nanoparticle, **(c)** AgNPs after the interaction with Pb^{2+} (16 ppm) and its fitted curve following equation (9) for absorption cross-section of nanoparticle and nanoparticle pair mixed system in ratio of 5:2, **(d)** AgNPs after the interaction with Pb^{2+} (23 ppm) and its fitted curve following equation (10) for absorption cross-section of nanoparticle and nanoparticle pair mixed system in ratio of 5:9.

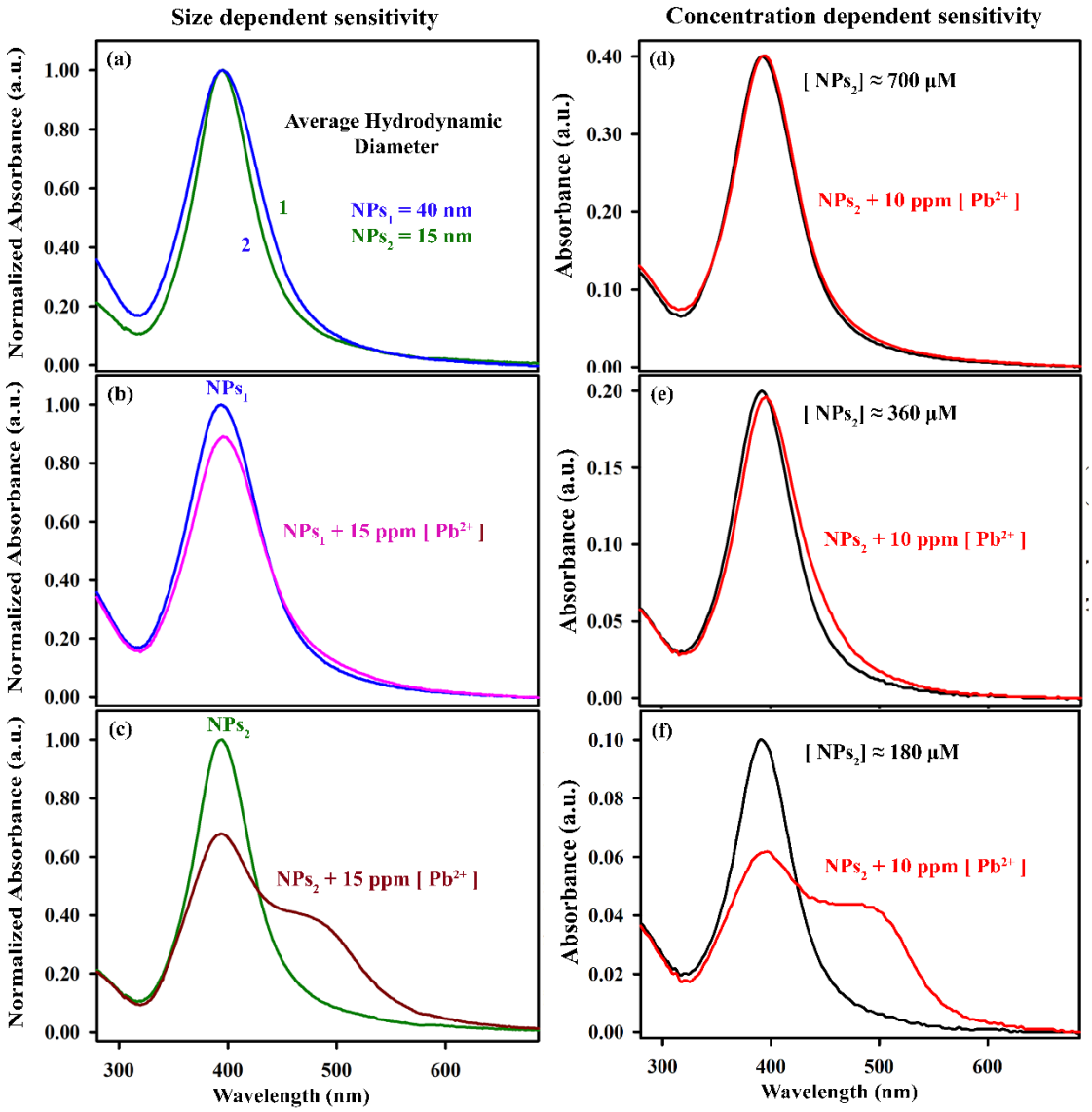

Fig. 4 (a) Normalized UV-Vis absorbance spectra of two sets of AgNPs, namely NPs_1 (Blue) and NPs_2 (Green) having a hydrodynamic diameter equal to 40 nm and 15 nm respectively. **(b, c)** Normalized UV-Vis absorbance spectra of the two AgNPs and their response i.e. NPs_1 (Pink) and NPs_2 (Dark Red) with 15 ppm of Pb^{2+}. The UV-vis absorbance spectra of AgNPs (having three different concentrations) in the absence (Black) and presence (Red) of Pb^{2+} (10 ppm) are shown in the panels (d-f). **(d, e, f)** Show the absorbance spectra of 700 µM, 360 µM and 180 µM concentration of NPs_2 at 10 ppm of Pb^{2+} respectively.

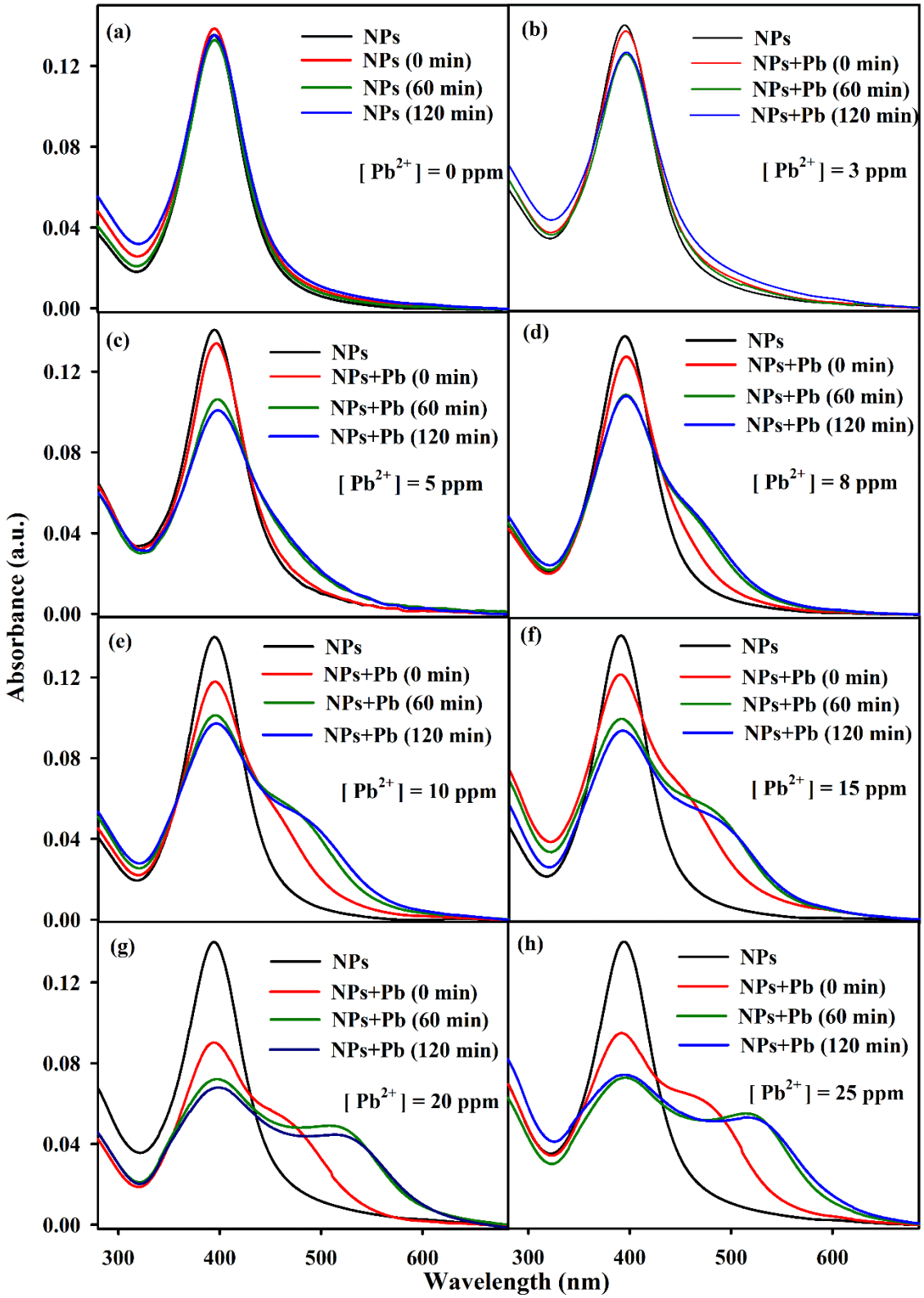

Fig. 5 Time dependent absorbance spectra of AgNPs colloidal solution at different concentrations of Pb^{2+} are shown in panels **(a-h)**. **(a)** Shows the variation of SPR in longer time window at [Pb^{2+}] = 0 ppm.

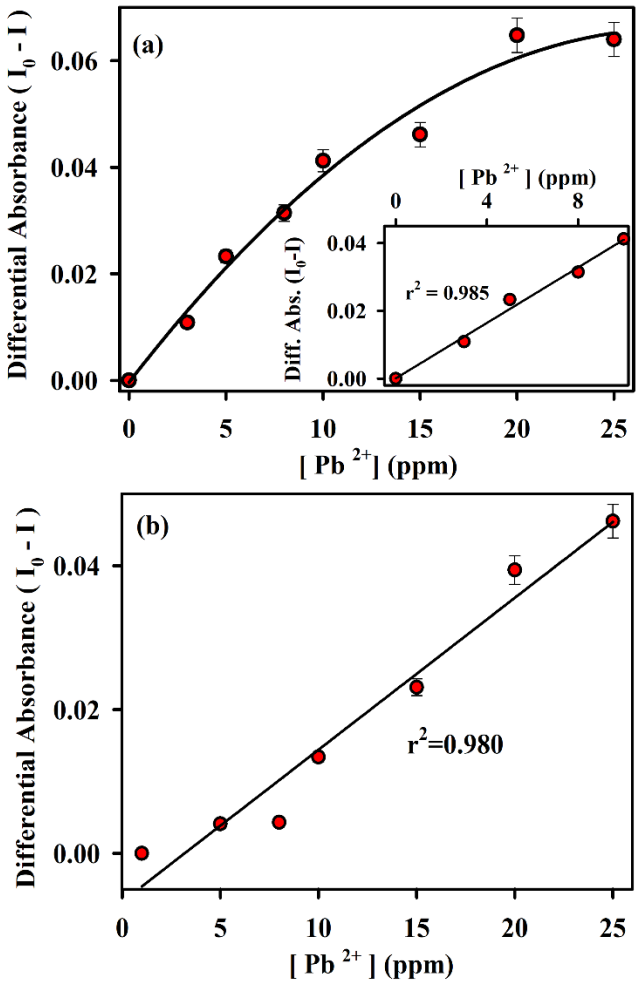

Fig. 6 (a) The differential absorbance spectra of the AgNPs solution at 395 nm with varying Pb^{2+} concentrations. Inset shows the linear response of the curve with [Pb^{2+}] ranging from 0 to 10 ppm. **(b)** Shows the plot of differential absorbance of the AgNPs solution at 520 nm with varying Pb^{2+} concentration.

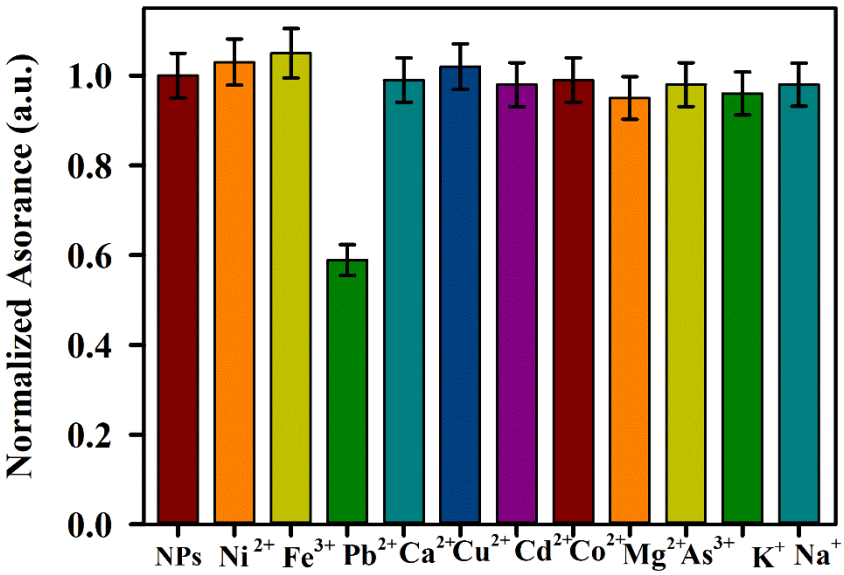

Fig. 7 Normalized UV-Vis absorbance spectra of the AgNPs colloidal solution monitored at 395 nm in the presence of various metal ions.

Table 1: List of parameters for ε_1 and ε_2 which best fit the equations (4), (9) and (10)

Parameters	Spectrum 1 (eq. (4))	Spectrum 2 (eq. (9))	Spectrum 3 (eq. (10))
A_1	-22.70±0.25	-23.86±0.86	-23.07±0.20
A_2	-725.33±8.80	-732.18±23.43	-1049.88±9.06
A_3	35.74±0.20	37.86±0.78	30.48±0.20
B_1	-0.18±1.05	-2.13±1.67	-0.84±0.46
B_2	8.02±5.74	15.75±7.92	7.75±1.51
B_3	656.32±546.24	640.65±396.82	620.06±172.34
C_1	0.41±0.00	0.41±0.00	0.41±0.00

Table of Content (Graphical Abstract)

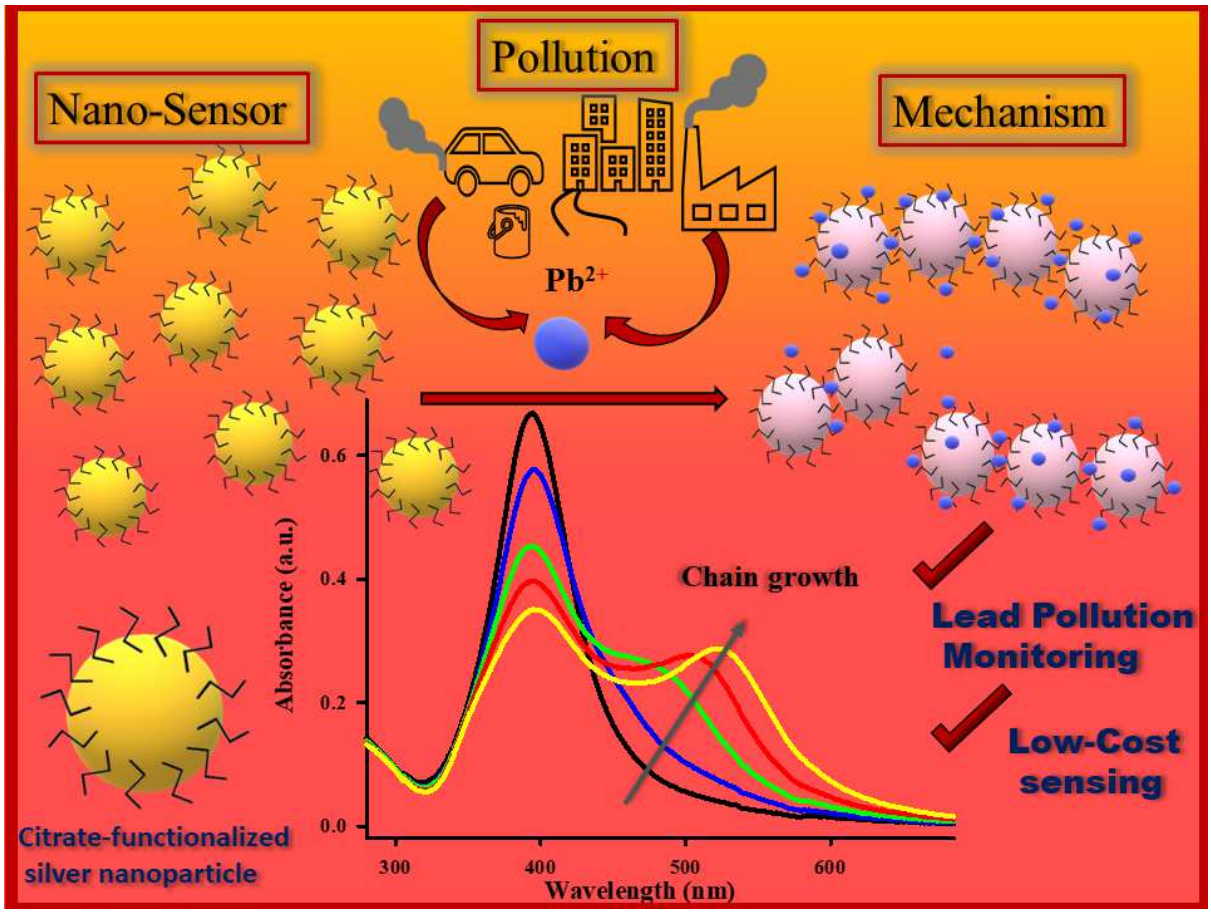

The possible sensing mechanism of citrate-functionalized silver nanoparticles towards Pb^{2+} followed by unique chain-like aggregation for potential atmospheric and industrial lead pollution monitoring.

Figures

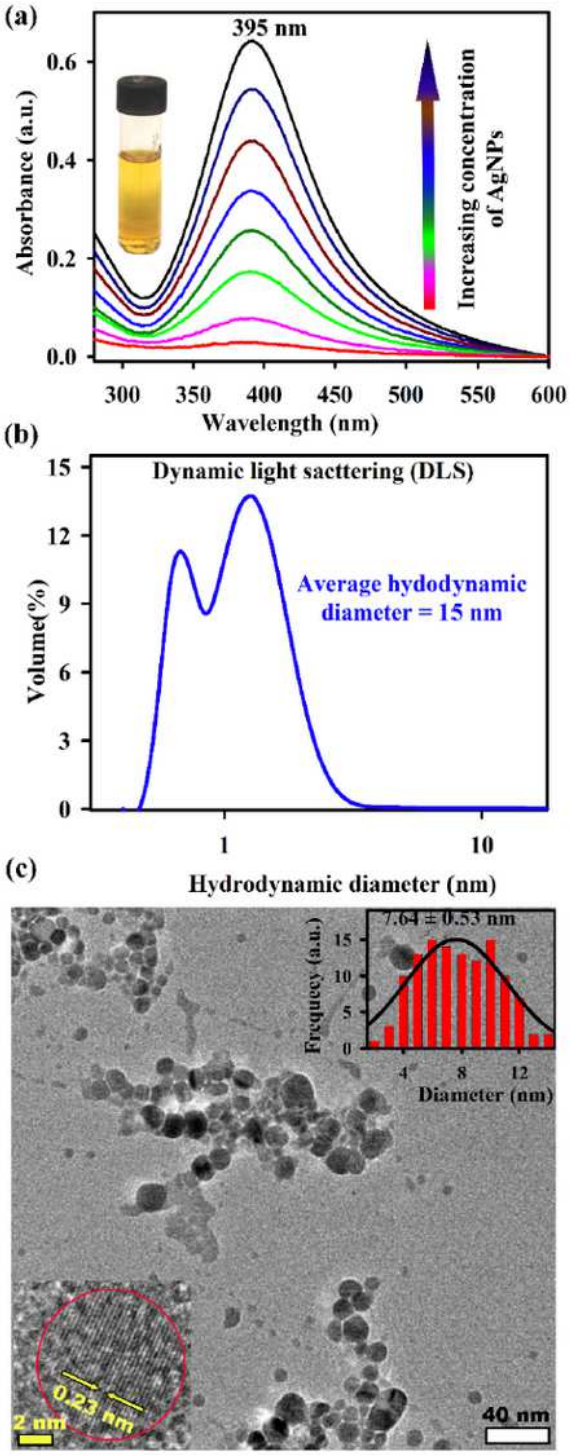

Figure 1

(a) UV–Vis absorbance spectra of citrate capped silver nanoparticle's (AgNPs) colloidal solution with varying concentration of AgNPs. The Inset shows the image of the colloidal solution. (b) Volume distribution of hydrodynamic diameter (axis in common logarithm) of AgNPs measured using Dynamic

Light Scattering. (c) TEM image of the AgNPs. Upper inset shows the size distribution of the AgNPs and lower inset shows a HRTEM image of the NP.

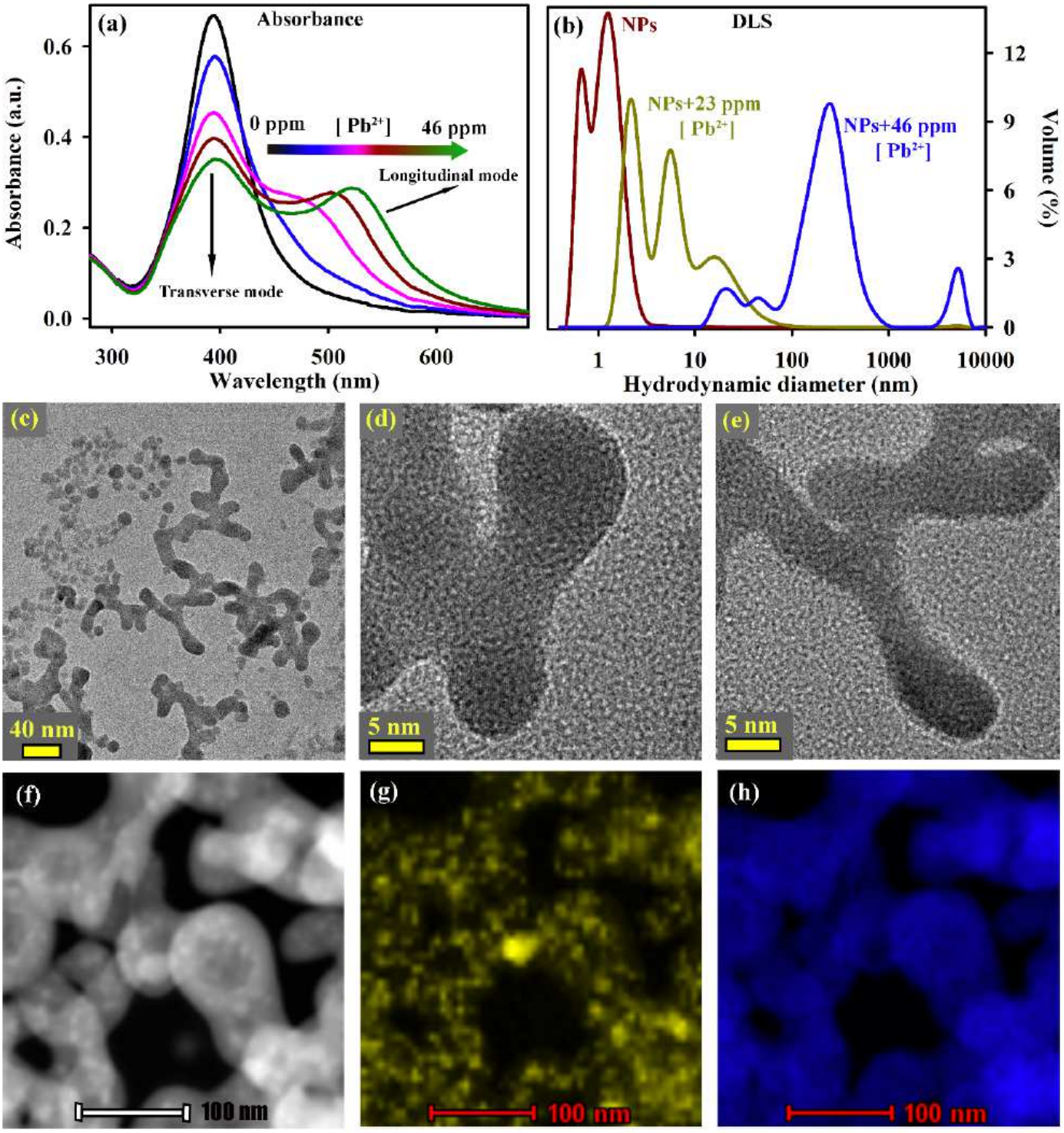

Figure 2

(a) UV-Vis absorbance spectra of AgNPs after interaction with Pb2+ in increasing order of concentration of Pb2+. (b) Volume distribution of hydrodynamic diameter of AgNPs (in Black) before and after interaction with two different concentrations of Pb2+ (in Green 23 ppm and Blue 46 ppm). (c) TEM image

of the AgNPs after interaction with Pb2+. (d, e) HRTEM images the AgNPs after the interaction with Pb2+, showing chain like geometry of the NPs of varying chain length. (f) Drift corrected spectrum image scanning display of lead added NP aggregates and its EFTEM compositional analysis are shown in panel (g, h). (g, h) Yellow and Blue represents the presence of silver and lead respectively.

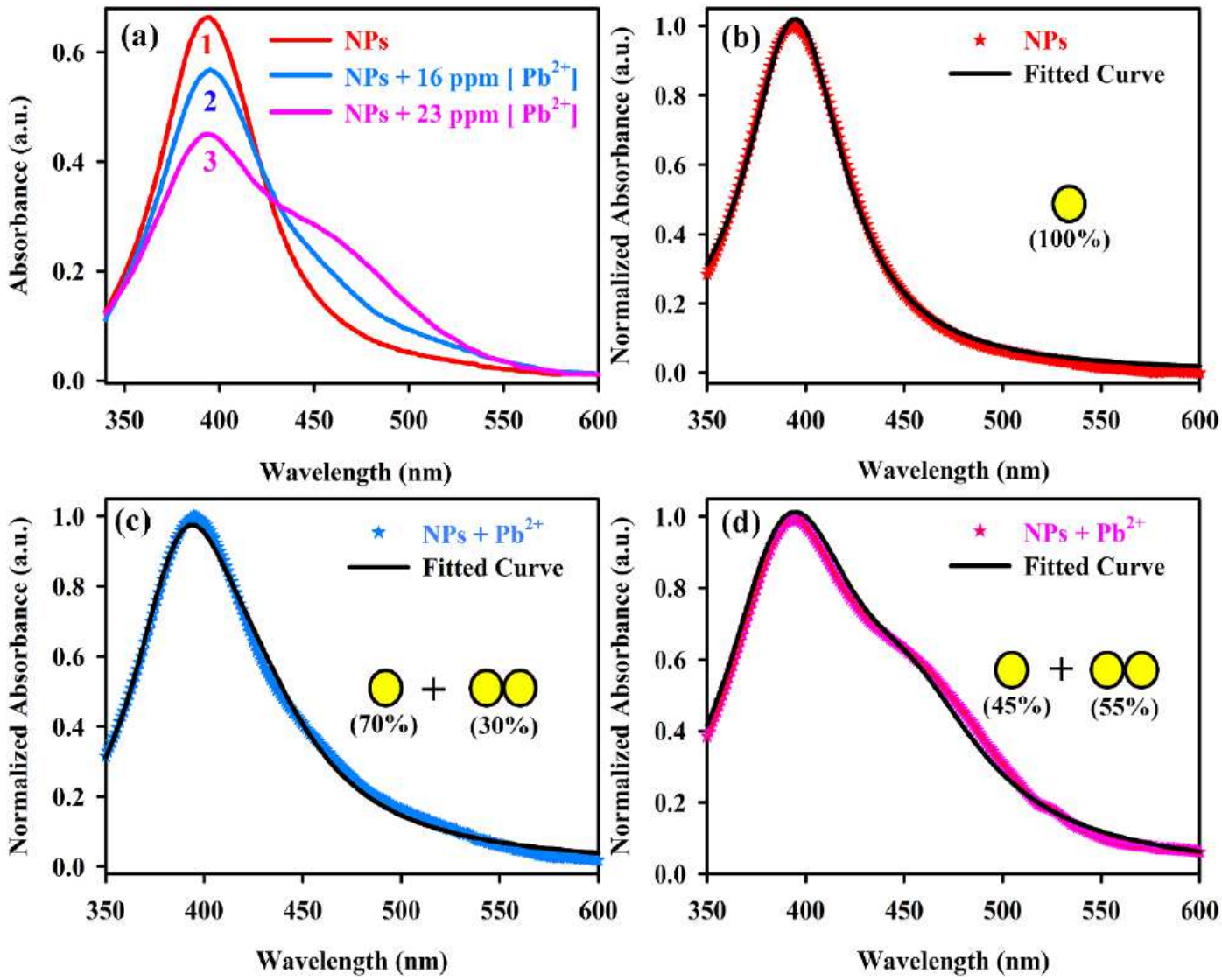

Figure 3

(a) UV-Vis absorbance spectra of AgNPs before (red) and after interaction with 16 ppm (Blue), 23 ppm (Pink) of Pb2+. The normalized UV-Vis absorbance spectra (as numbered in (a)) and the fitted curve (in Black) based on their corresponding equation for absorption cross-section equations are represented in panels from (b-d). The normalized UV-Vis absorbance spectra of (b) AgNPs before interaction with Pb2+ and its fitted curve following equation (4) for absorption cross-section of nanoparticle, (c) AgNPs after the interaction with Pb2+ (16 ppm) and its fitted curve following equation (9) for absorption cross-section of nanoparticle and nanoparticle pair mixed system in ratio of 5:2, (d) AgNPs after the interaction with Pb2+ (23 ppm) and its fitted curve following equation (10) for absorption cross-section of nanoparticle and nanoparticle pair mixed system in ratio of 5:9.

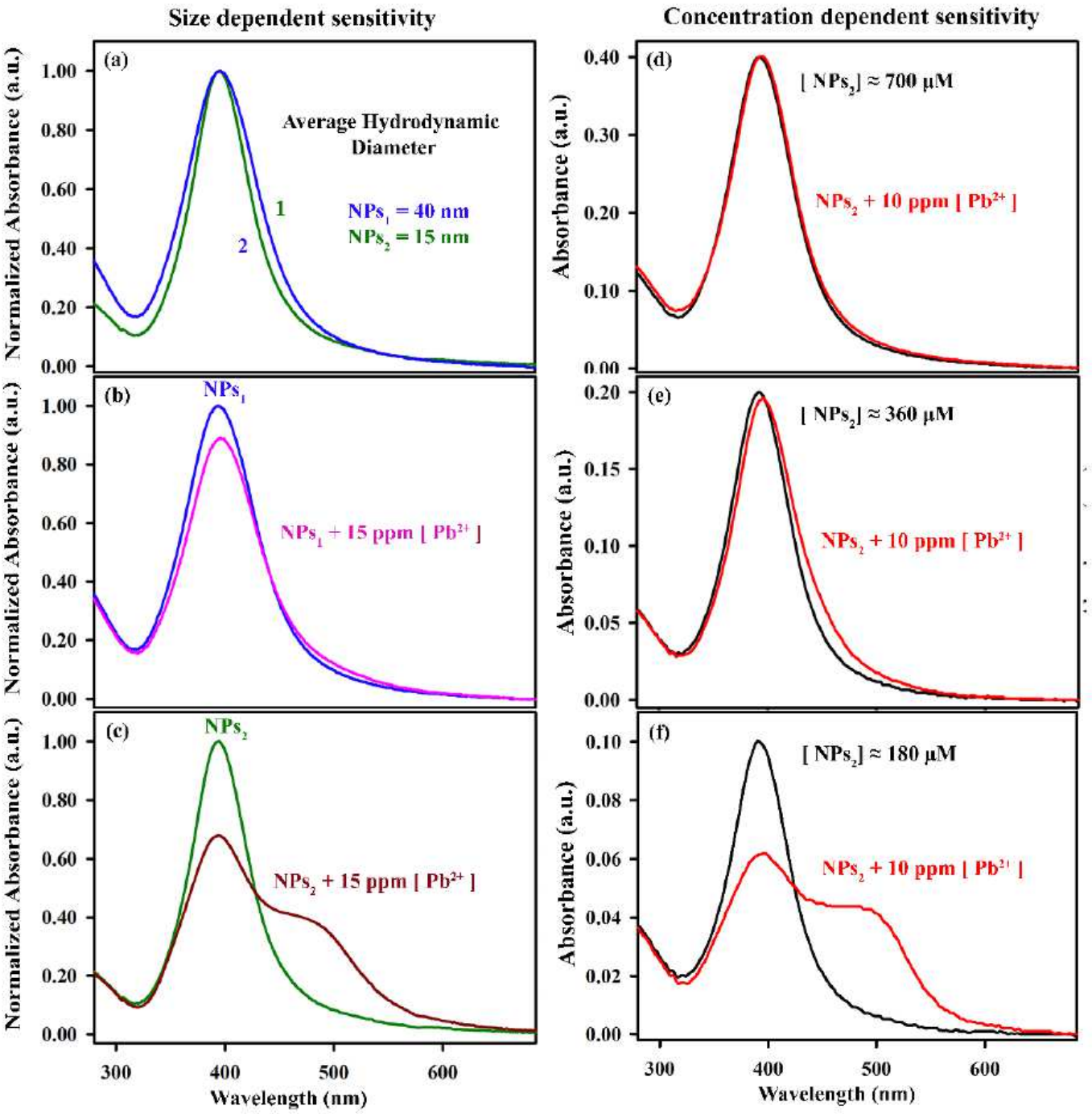

Figure 4

(a) Normalized UV-Vis absorbance spectra of two sets of AgNPs, namely NPs1 (Blue) and NPs2 (Green) having a hydrodynamic diameter equal to 40 nm and 15 nm respectively. (b, c) Normalized UV-Vis absorbance spectra of the two AgNPs and their response i.e. NPs1 (Pink) and NPs2 (Dark Red) with 15 ppm of Pb2+. The UV-vis absorbance spectra of AgNPs (having three different concentrations) in the absence (Black) and presence (Red) of Pb2+ (10 ppm) are shown in the panels (d-f). (d, e, f) Show the absorbance spectra of 700 µM, 360 µM and 180 µM concentration of NPs2 at 10 ppm of Pb2+ respectively.

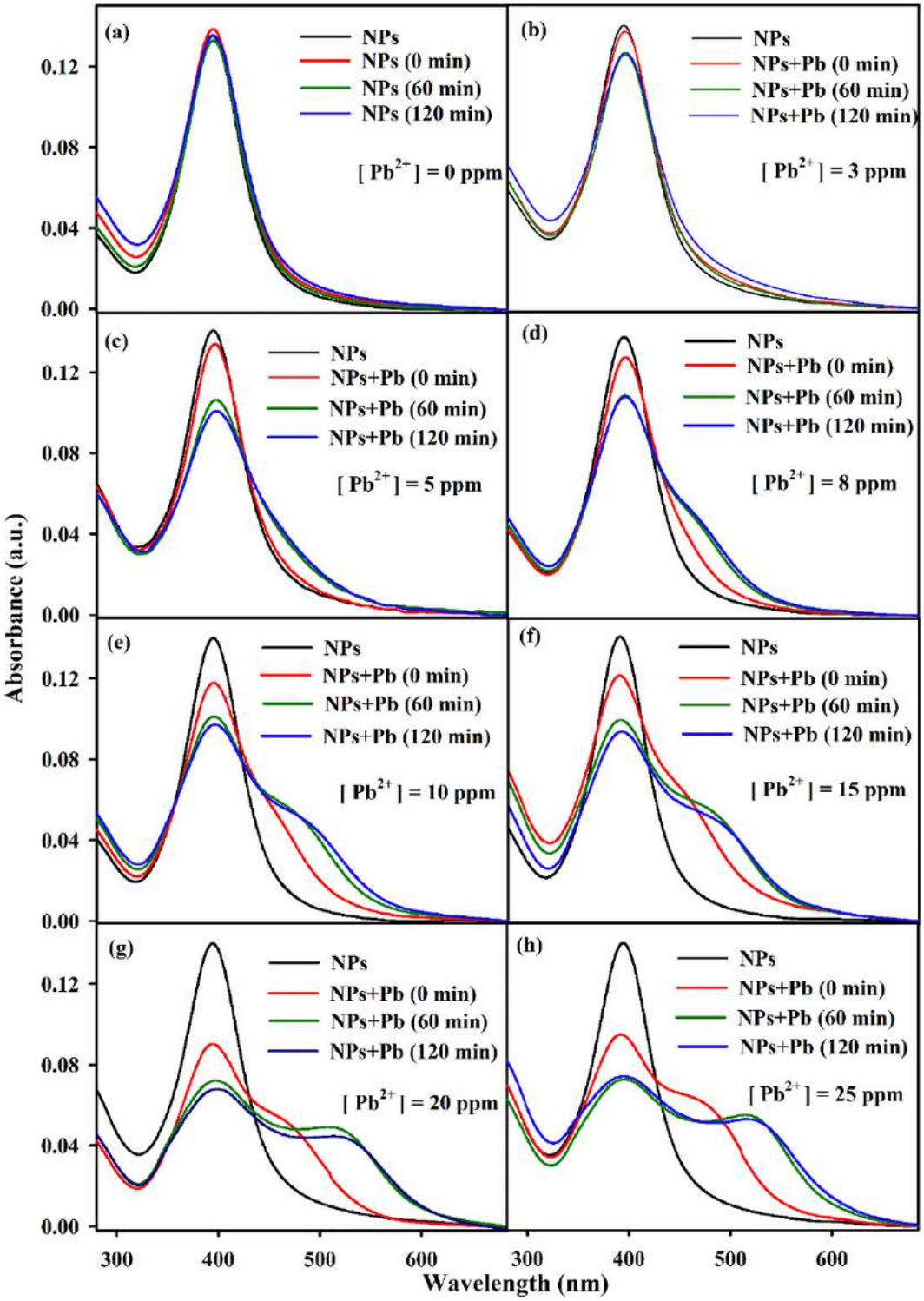

Figure 5

Time dependent absorbance spectra of AgNPs colloidal solution at different concentrations of Pb2+ are shown in panels (a-h). (a) Shows the variation of SPR in longer time window at [Pb2+] = 0 ppm.

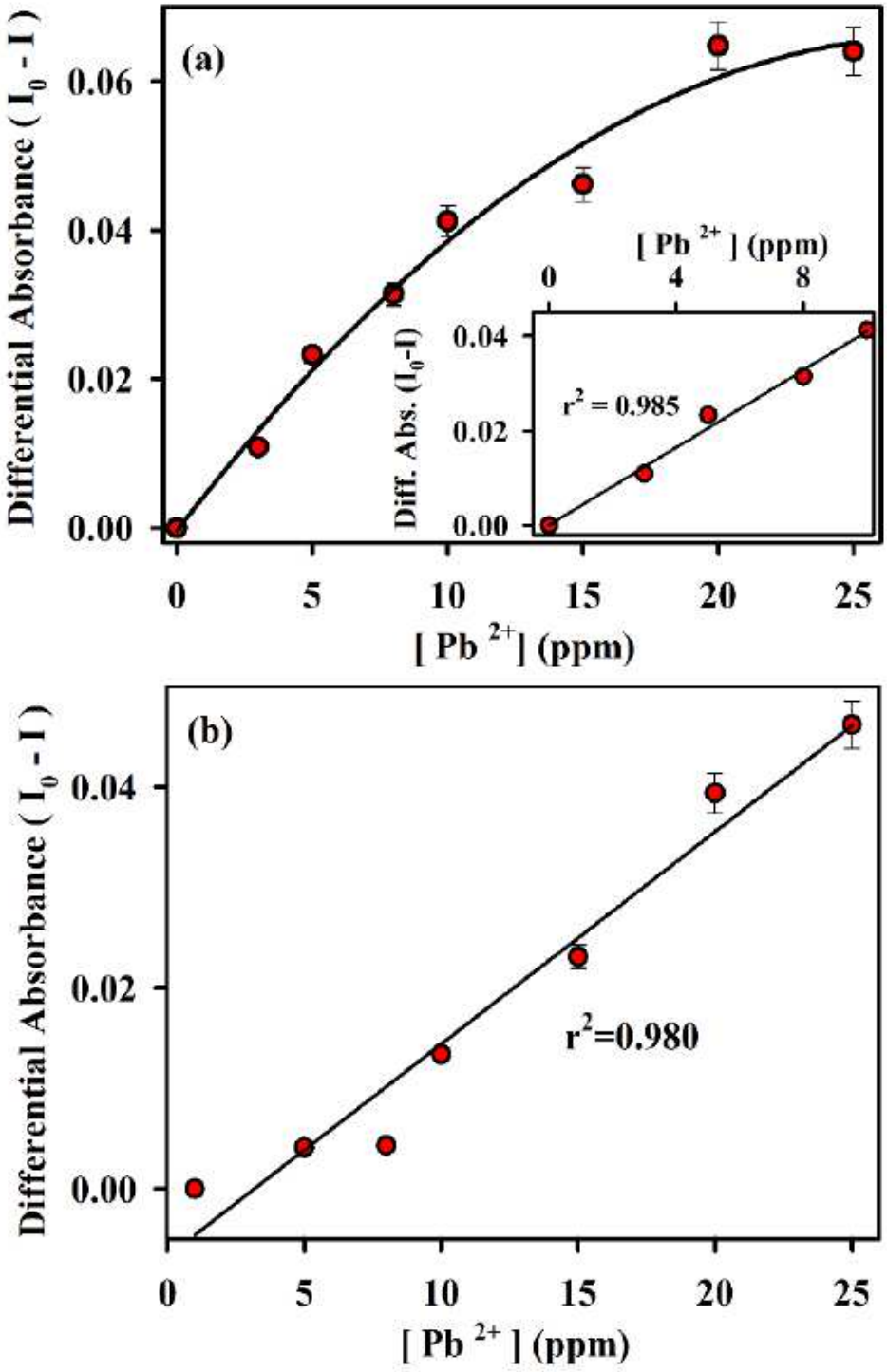

Figure 6

(a) The differential absorbance spectra of the AgNPs solution at 395 nm with varying Pb2+ concentrations. Inset shows the linear response of the curve with [Pb2+] ranging from 0 to 10 ppm. (b) Shows the plot of differential absorbance of the AgNPs solution at 520 nm with varying Pb2+ concentration.

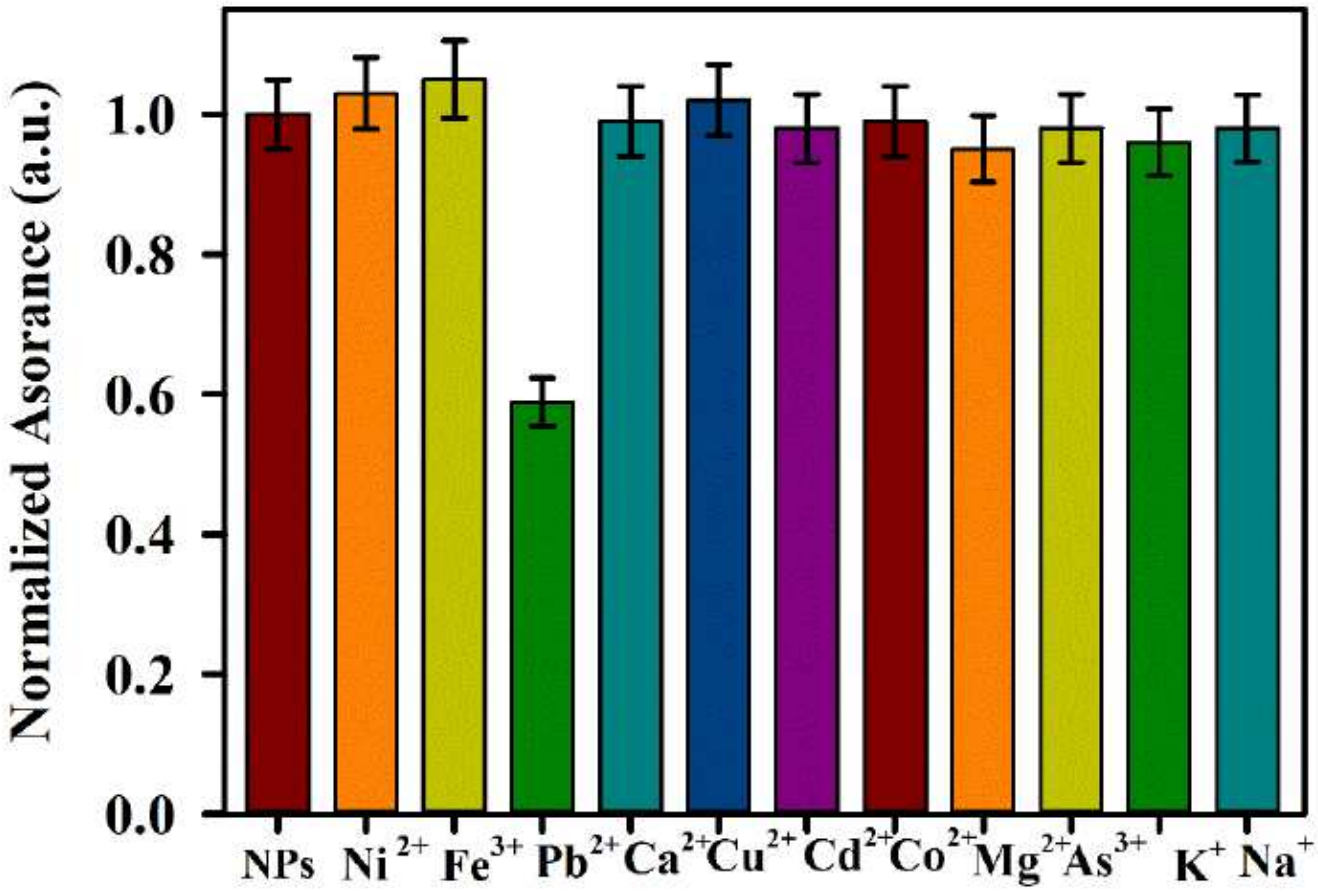

Figure 7

Normalized UV-Vis absorbance spectra of the AgNPs colloidal solution monitored at 395 nm in the presence of various metal ions.

Supplementary Files

This is a list of supplementary files associated with this preprint. Click to download.

- GraphicalAbstract.png